In-gap electronic states of GeAsSe and SiGeAsSe alloys for selector devices from atomistic simulations
Supporting Information

Sebastiano Caravati,[a] Dario Baratella,[a] Paolo Fantini,[b] Marco Bernasconi[a]
[a] *Department of Materials Science, University of Milano-Bicocca, Via R. Cozzi 55, I-20125, Milano, Italy and*
[b] *Micron Technology Inc., Via Trento, 26, I-20871, Vimercate, Italy*

model	Ge_t	with Ge	As	Se	total
$Ge_{25}As_{30}Se_{45}$	36 %				
(120 ps)	Ge	0.16	0.44	2.79	3.39
	As	0.37	1.40	1.23	3.00
	Se	1.55	0.82	–	2.37
$Ge_{25}As_{30}Se_{45}$	23 %				
(40 ps)	Ge	0.05	0.35	2.85	3.25
	As	0.29	1.53	1.22	3.04
	Se	1.59	0.81	0.04	2.44
$Ge_{25}As_{30}Se_{45}$	33 %				
(12 ps)	Ge	0.21	0.49	2.63	3.33
	As	0.41	1.29	1.30	3.00
	Se	1.46	0.87	0.04	2.37
$Ge_{15}As_{34}Se_{51}$	40 %				
(120 ps)	Ge	0.04	0.47	3.00	3.51
	As	0.21	0.94	1.87	3.02
	Se	0.88	1.25	0.07	2.20
$Ge_{15}As_{34}Se_{51}$	44 %				
(40 ps)	Ge	0.09	0.31	3.16	3.56
	As	0.14	1.06	1.80	3.00
	Se	0.93	1.20	0.05	2.18
$Ge_{15}As_{34}Se_{51}$	49 %				
(12 ps)	Ge	0.04	0.51	2.93	3.49
	As	0.23	1.08	1.72	3.02
	Se	0.86	1.14	0.12	2.12
$Ge_{15}As_{34}Se_{51}$	40 %				
(6 ps)	Ge	0.00	0.47	2.96	3.42
	As	0.21	1.06	1.72	2.98
	Se	0.87	1.14	0.16	2.17
$Ge_{25}As_{20}Se_{55}$	36 %				
(120 ps)	Ge	0.08	0.19	3.13	3.40
	As	0.23	0.53	2.23	3.00
	Se	1.42	0.81	0.07	2.31
$Ge_{25}As_{20}Se_{55}$	43 %				
(40 ps)	Ge	0.13	0.27	3.07	3.47
	As	0.33	0.43	2.23	3.00
	Se	1.39	0.81	0.07	2.28
$Ge_{25}As_{20}Se_{55}$	36 %				
(12 ps)	Ge	0.21	0.28	2.91	3.40
	As	0.35	0.27	2.43	3.05
	Se	1.32	0.88	0.10	2.30
$Ge_{12.5}As_{25}Se_{62.5}$	68 %				
(120 ps)	Ge	0.11	0.24	3.34	3.68
	As	0.12	0.13	2.76	3.01
	Se	0.67	1.11	0.29	2.07
$Ge_{12.5}As_{25}Se_{62.5}$	63 %				
(40 ps)	Ge	–	0.13	3.53	3.66
	As	0.07	0.37	2.59	3.03
	Se	0.71	1.04	0.35	2.09
$Ge_{12.5}As_{25}Se_{62.5}$	32 %				
(12 ps)	Ge	0.11	0.13	3.13	3.37
	As	0.07	0.45	2.47	2.99
	Se	0.63	0.99	0.53	2.14
$Ge_{25}As_{10}Se_{65}$	59 %				
(120 ps)	Ge	0.03	0.03	3.60	3.65
	As	0.07	0.07	2.87	3.00
	Se	1.38	0.44	0.37	2.19
$Ge_{25}As_{10}Se_{65}$	49 %				
(40 ps)	Ge	0.05	0.05	3.44	3.55
	As	0.13	0.07	2.80	3.00
	Se	1.32	0.43	0.47	2.23
$Ge_{25}As_{10}Se_{65}$	41 %				
(12 ps)	Ge	0.03	0.07	3.37	3.47
	As	0.17	0.07	2.77	3.00
	Se	1.30	0.43	0.52	2.25

TABLE I: Fraction of Ge atoms in tetrahedral environment (Ge_t) and average coordination numbers for different pairs of atoms computed from the partial pair correlation functions for the $Ge_xAs_ySe_{100-x-y}$ models generated by quenching from the melt with different quenching times.

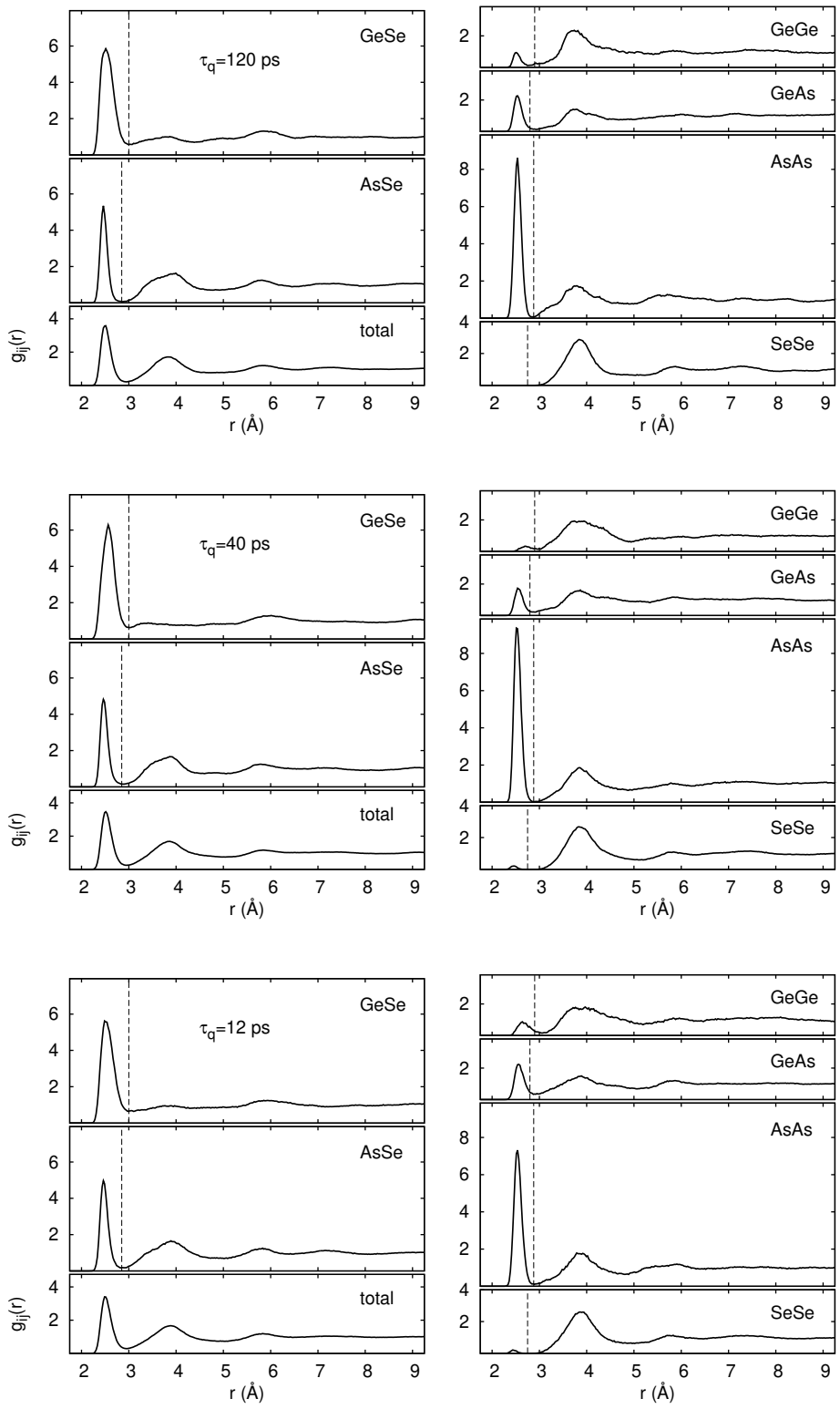

Figure S1. Pair correlation functions of a-$Ge_{25}As_{30}Se_{45}$ generated by quenching from the melt in 120, 40 and 12 ps.

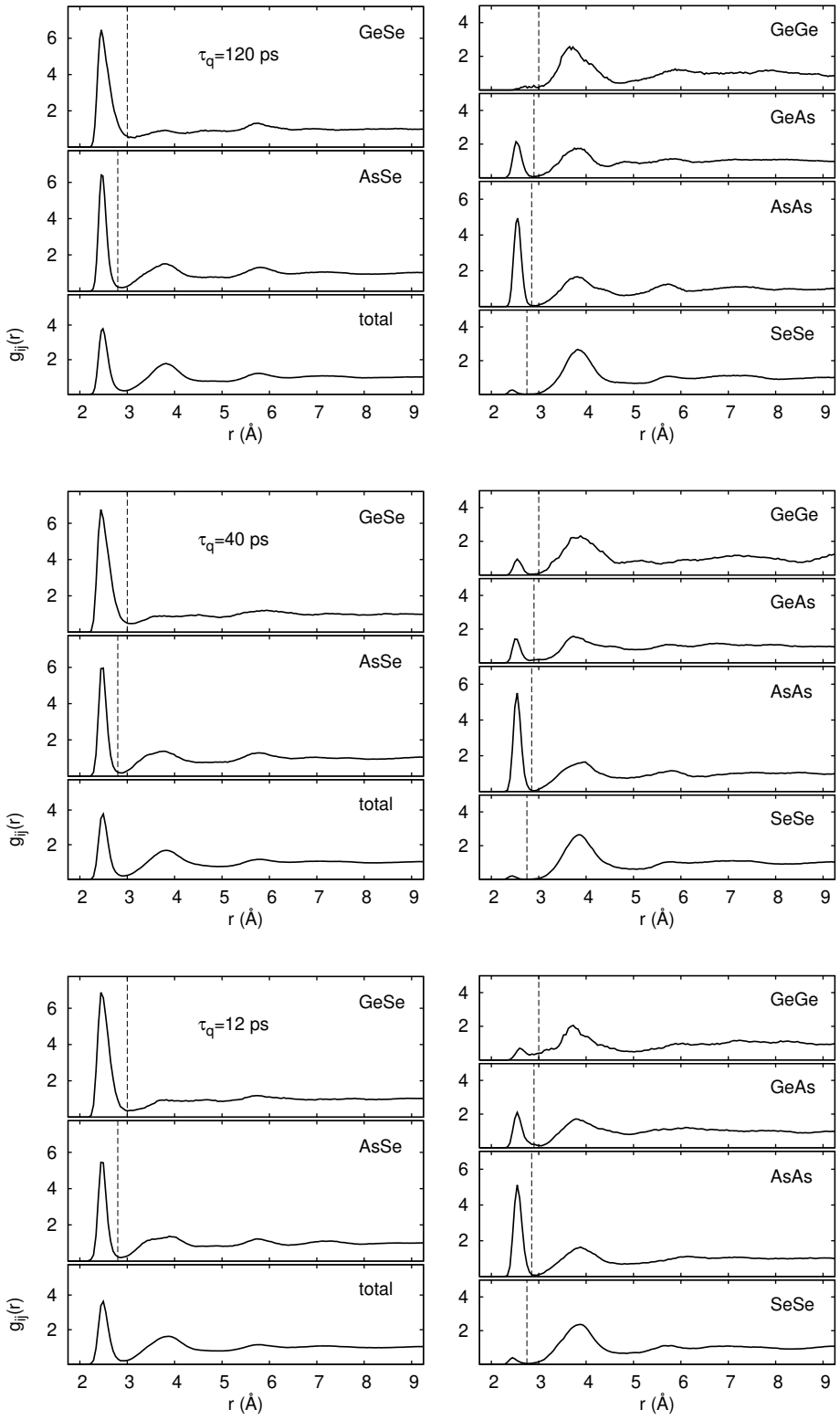

Figure S2. Pair correlation functions of a-$Ge_{15}As_{34}Se_{51}$ generated by quenching from the melt in 120, 40 and 12 ps.

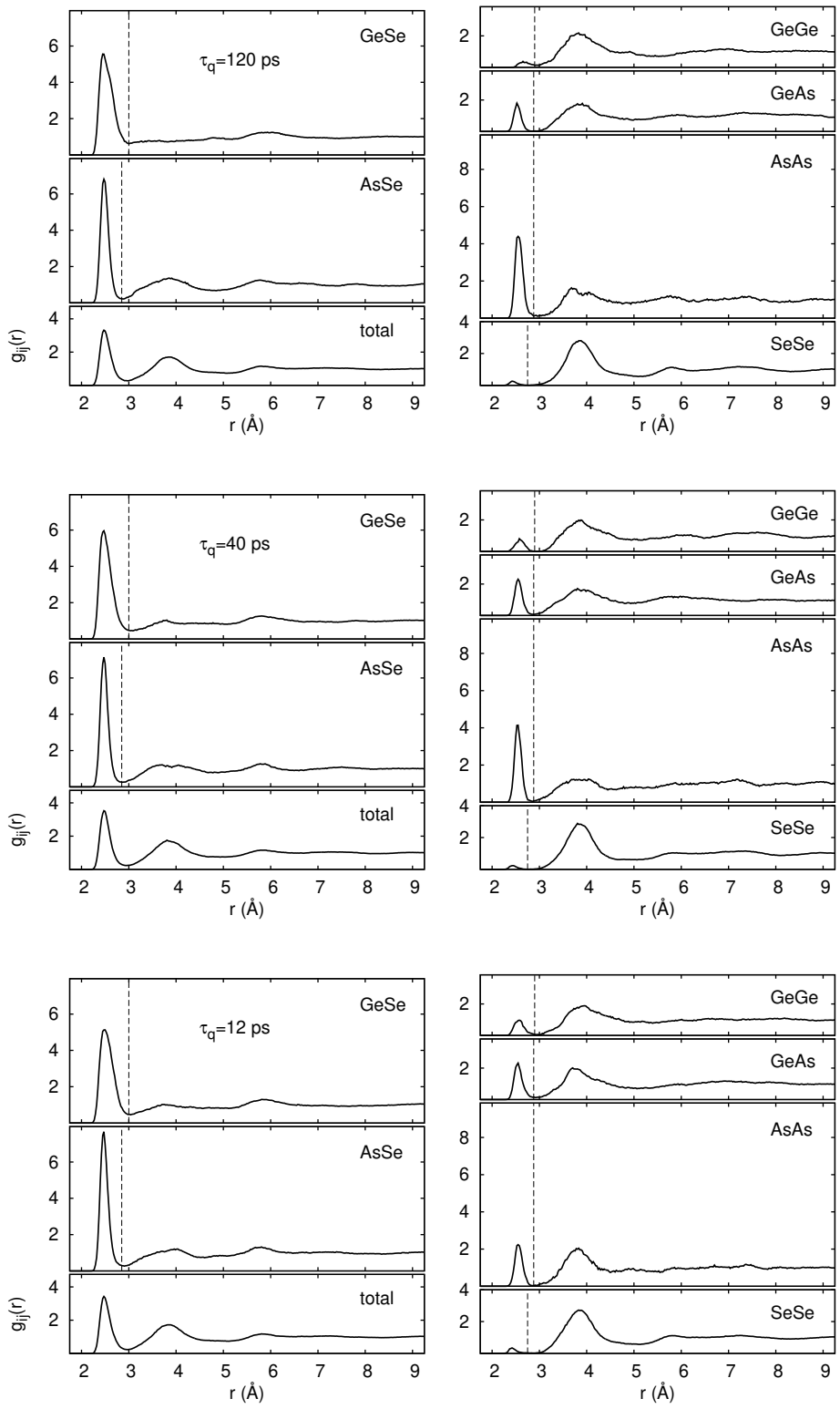

Figure S3. Pair correlation functions of a-$Ge_{25}As_{20}Se_{55}$ generated by quenching from the melt in 120, 40 and 12 ps.

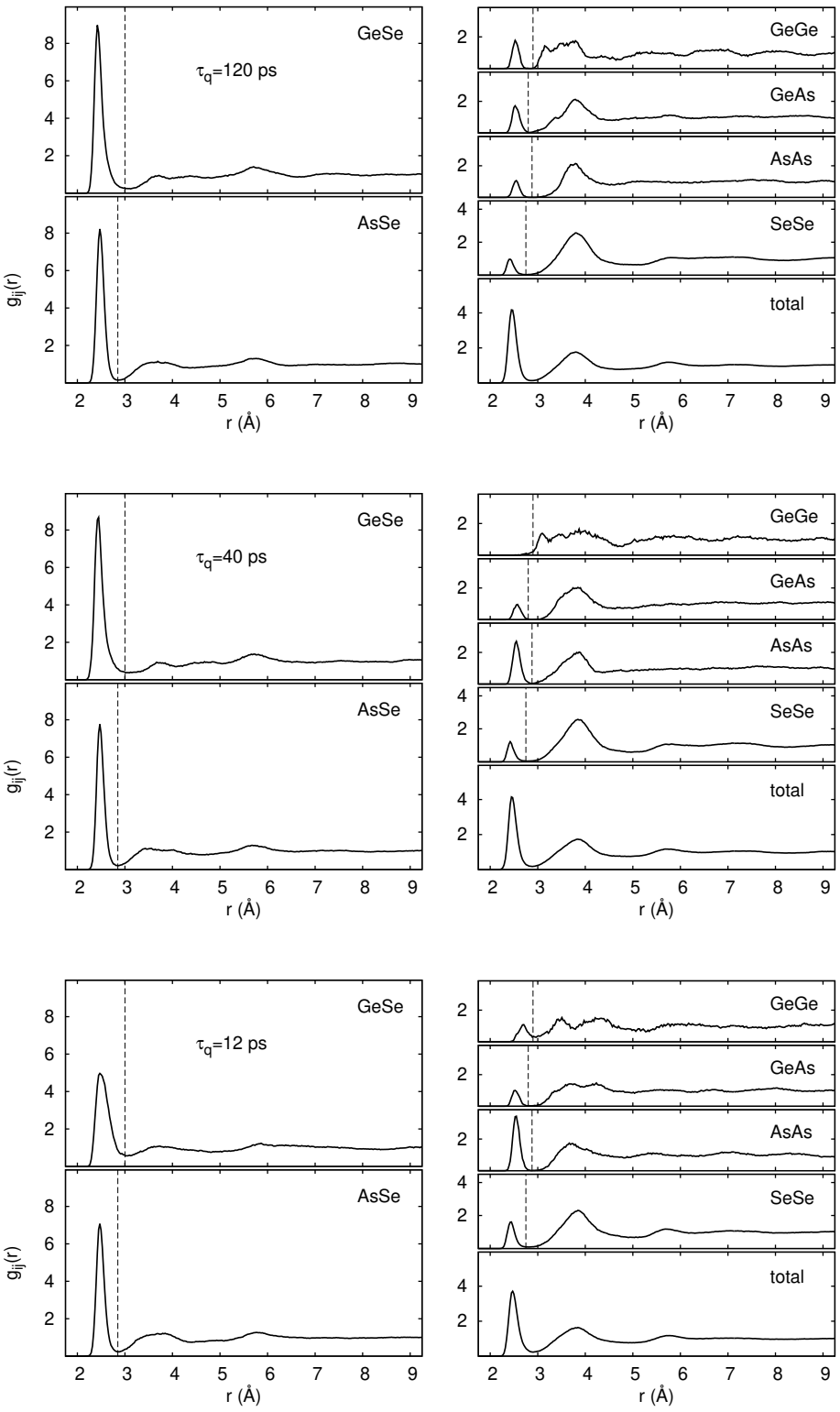

Figure S4. Pair correlation functions of a-$Ge_{12.5}As_{25}Se_{62.5}$ generated by quenching from the melt in 120, 40 and 12 ps.

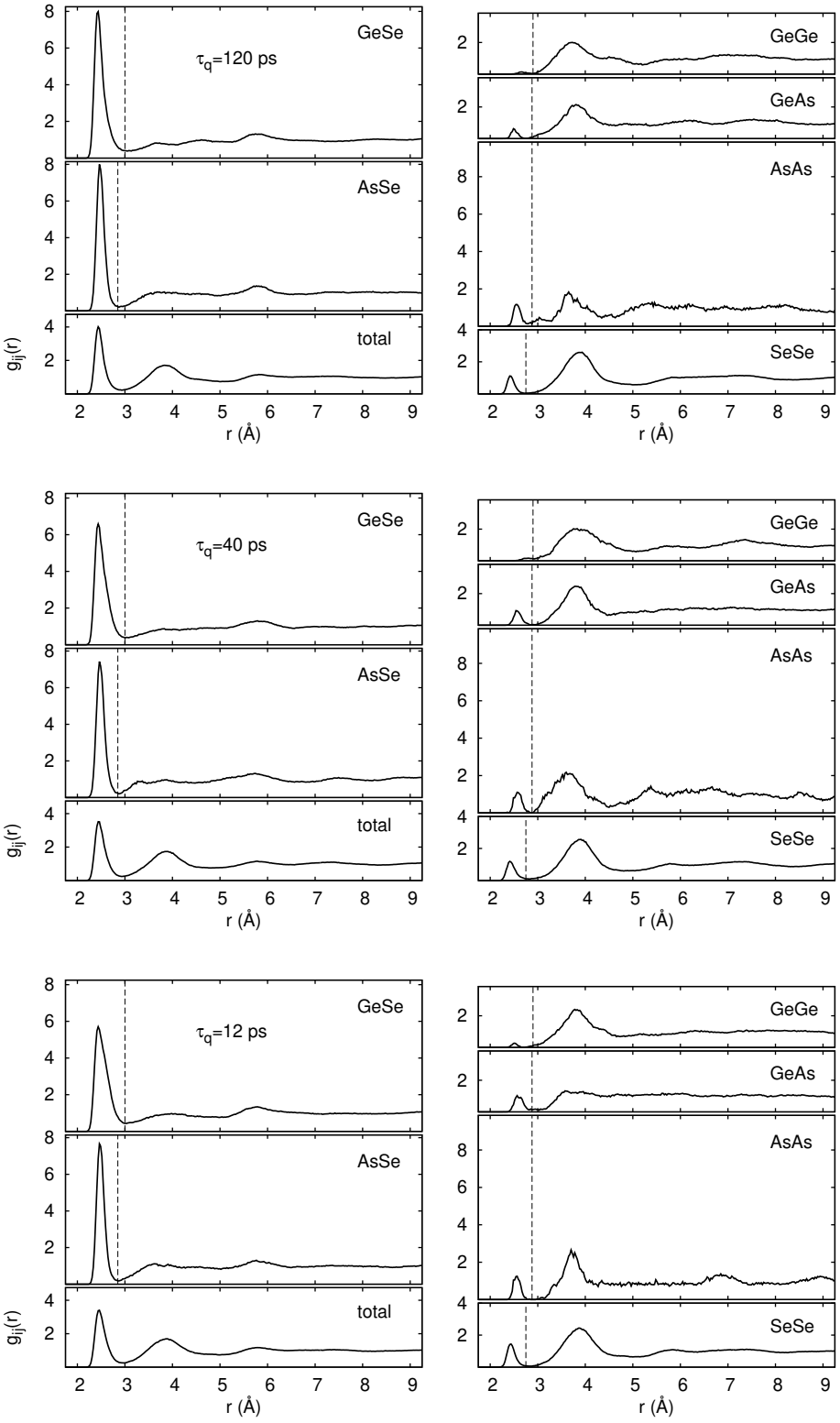

Figure S5. Pair correlation functions of a-$Ge_{25}As_{10}Se_{65}$ generated by quenching from the melt in 120, 40 and 12 ps.

$Ge_{15}As_{34}Se_{51}$	Method	GeGe	GeAs	GeSe	AsGe	AsAs	AsSe	SeGe	SeAs	SeSe
This Work	DFT	0.04	0.47	3.00	0.21	0.94	1.87	0.88	1.25	0.07
$Ge_{15}As_{34}Se_{51}$ [1]	RMC	0.64	1.61	1.66	0.71	1.15	1.06	0.49	0.71	0.84
$Ge_{25}As_{20}Se_{55}$	Method	GeGe	GeAs	GeSe	AsGe	AsAs	AsSe	SeGe	SeAs	SeSe
This Work	DFT	0.08	0.19	3.13	0.23	0.53	2.23	1.42	0.81	0.07
$Ge_{21}As_{21}Se_{58}$ [3]	DFT	0.08	0.35	3.37	0.35	0.65	1.97	1.22	0.71	0.12
$Ge_{22}As_{20}Se_{58}$ [2]	RMC	1.46	0.88	1.69	0.96	0.66	1.41	0.64	0.48	0.93
$Ge_{12.5}As_{25}Se_{62.5}$	Method	GeGe	GeAs	GeSe	AsGe	AsAs	AsSe	SeGe	SeAs	SeSe
This Work	DFT	0.11	0.24	3.34	0.12	0.13	2.76	0.67	1.11	0.29
$Ge_{12.5}As_{25}Se_{62.5}$ [4]	DFT	0.02	0.18	3.33	0.10	0.30	2.63	0.65	1.05	0.40
$Ge_{15}As_{25}Se_{60}$ [1]	RMC	1.07	1.19	1.74	0.71	0.83	1.48	0.44	0.62	1.03
$Ge_{25}As_{10}Se_{65}$	Method	GeGe	GeAs	GeSe	AsGe	AsAs	AsSe	SeGe	SeAs	SeSe
This Work	DFT	0.03	0.03	3.60	0.07	0.07	2.87	1.38	0.44	0.37
$Ge_{25}As_{10}Se_{65}$ [5]	DFT	0.16	0.07	3.11	0.00	0.18	2.87	1.20	0.44	0.57
$Ge_{22.5}As_{25}Se_{67.5}$ [2]	RMC	1.68	0.52	1.82	1.18	0.36	1.49	0.61	0.22	1.16
$Ge_{27.5}As_{25}Se_{62.5}$ [2]	RMC	1.84	0.47	1.72	1.30	0.30	1.42	0.76	0.23	1.02

Table SII. Coordination numbers of a-$Ge_{12.5}As_{25}Se_{62.5}$, a-$Ge_{25}As_{20}Se_{55}$, a-$Ge_{25}As_{10}Se_{65}$, and a-$Ge_{15}As_{34}Se_{51}$ compared with previous DFT models and RMC models obtained by fitting experimental diffraction data with similar compositions. The discrepancy between our results and previous DFT data [5] for the $Ge_{25}As_{20}Se_{65}$ alloy mostly comes from a different choice of the bonding cutoff.

$Ge_{15}As_{34}Se_{51}$	Method	GeGe	GeAs	GeSe	AsAs	AsSe	SeSe
This Work	DFT	2.55	2.52	2.45	2.55	2.45	2.45
$Ge_{15}As_{34}Se_{51}$ [1]	RMC	2.38	2.45	2.33	2.43	2.37	2.36
$Ge_{25}As_{20}Se_{55}$	Method	GeGe	GeAs	GeSe	AsAs	AsSe	SeSe
This Work	DFT	2.58	2.52	2.45	2.55	2.47	2.42
$Ge_{22}As_{20}Se_{58}$ [2]	RMC	2.38	2.45	2.36	2.40	2.39	2.35
$Ge_{12.5}As_{25}Se_{62.5}$	Method	GeGe	GeAs	GeSe	AsAs	AsSe	SeSe
This Work	DFT	2.52	2.52	2.42	2.55	2.47	2.42
$Ge_{15}As_{25}Se_{60}$ [1]	RMC	2.37	2.44	2.34	2.40	2.40	2.37
$Ge_{25}As_{10}Se_{65}$	Method	GeGe	GeAs	GeSe	AsAs	AsSe	SeSe
This Work	DFT	2.52	2.49	2.44	2.54	2.46	2.41
$Ge_{22.5}As_{25}Se_{67.5}$ [2]	RMC	2.36	2.45	2.37	2.35	2.39	2.33
$Ge_{27.5}As_{25}Se_{62.5}$ [2]	RMC	2.40	2.45	2.35	2.41	2.37	2.36

Table SIII. Nearest neighbors distances (from the first peak of the partial pair correlation functions) of a-$Ge_{12.5}As_{25}Se_{62.5}$, a-$Ge_{25}As_{20}Se_{55}$, a-$Ge_{25}As_{10}Se_{65}$, and a-$Ge_{15}As_{34}Se_{51}$ compared with previous DFT models and RMC models obtained by fitting experimental diffraction data with similar compositions.

composition	τ_q (ps)	AsSe (%)	GeSe	AsAs	GeAs	SeSe	GeGe
$Ge_{25}As_{30}Se_{45}$	120	26	49.5	15	8	–	1.4
≫	40	26	50.5	16	6	0.7	0.5
≫	12	28	47	14	9	0.7	1.9
$Ge_{15}As_{34}Se_{51}$	120	48	34	12	5	1	0.3
≫	40	46	36	14	3.5	1	0.5
≫	12	44	33	14	6	2	0.3
≫	6	44	34	14	5	3	–
$Ge_{25}As_{20}Se_{55}$	120	33	58	4	3	1.5	0.7
≫	40	33	56	3	5	1.5	1.2
≫	12	37	53	2	5	2	2
$Ge_{12.5}As_{25}Se_{62.5}$	120	55	33	1.3	2	7	0.5
≫	40	51	35	3.7	1.3	9	–
≫	12	49	31	4.5	1.3	13	0.5
$Ge_{25}As_{10}Se_{65}$	120	22	68	0.3	0.5	9	0.3
≫	40	21	65	0.3	1	12	0.5
≫	12	21	64	0.3	1.3	13	0.3

Table SIV. Percentage of the different types of bonds in the models of amorphous $Ge_xAs_ySe_{100-x-y}$ generated by quenching from the melt with different quenching times τ_q.

composition	τ_q (ps)	Ge_t (%)	abs. number	Ge_t with wrong bonds	isolated Ge_t	corner sh. couples	edge sh. couples
$Ge_{25}As_{30}Se_{45}$	120	36	27	25	9	15	0
≫	40	23	17	13	9	2	2
≫	12	32	24	23	10	9	0
$Ge_{15}As_{34}Se_{51}$	120	40	18	11	11	5	0
≫	40	44	20	13	7	8	1
≫	12	49	22	16	11	6	1
≫	6	40	18	13	10	5	0
$Ge_{25}As_{20}Se_{55}$	120	36	27	16	8	11	1
≫	40	43	32	23	14	13	2
≫	12	35	26	21	9	10	0
$Ge_{12.5}As_{25}Se_{62.5}$	120	68	26	11	14	5	2
≫	40	63	24	5	9	7	2
≫	12	32	12	6	12	–	–
$Ge_{25}As_{10}Se_{65}$	120	57	43	3	6	24	3
≫	40	49	37	6	8	20	2
≫	12	41	31	6	10	14	1
$Si_{10}Ge_{15}As_{30}Se_{45}$	120	35	26	24	11	7	3
≫	40	28	21	19	14	4	–
≫	12	36	27	24	13	8	1

Table SV. Statistics of Ge atoms in tetrahedral environment (Ge_t) in the models at different compositions and for different quenching times.

	2	3	4
Ge:	5.2 Se_2: 5.2	86.2 Se_3: 69.0 $AsSe_2$: 12.1 Ge^tSe_2: 3.4 As_2Se: 1.7	8.6 Se_4: 8.6
Ge^t: (23 %)	—	—	100 $AsSe_3$: 35.3 Se_4: 23.5 As_2Se_2: 23.5 $GeSe_3$: 11.8 As_3Se: 5.9
As:	—	95.5 As_2Se: 31.1 $AsSe_2$: 22.2 As_3: 13.3 Se_3: 7.8 Ge^tAs_2: 5.6 Ge^tSe_2: 4.4 Ge^tAsSe: 4.4 GeAsSe: 3.3 $GeAs_2$: 2.2 Ge^t_2Se: 1.1	4.4 Ge^tAsSe_2: 1.1 Ge^tGeAs_2: 1.1 Ge_3As: 1.1 $AsSe_3$: 1.1
Se:	56.3 GeAs: 17.0 As_2: 12.6 Ge^tGe: 10.4 Ge^tAs: 7.4 Ge^t_2: 3.7 Ge_2: 2.2 AsSe: 1.5 GeSe: 1.5	43.0 Ge_2As: 15.6 Ge_3: 10.4 Ge^tGe_2: 6.7 Ge^tGeAs: 4.4 $GeAs_2$: 4.4 Ge_2Se: 1.5	0.7 Ge_2As_2: 0.7

Table SVI. Statistics of coordination environments in a-$Ge_{25}As_{30}Se_{45}$ quenched in 40 ps. The percentage of the total number of atoms of each element is given for configurations with a weight greater than 1 %.

	2	3	4
Ge:	4.0	90.0	6.0
	Se_2: 2.0	Se_3: 62.0	Se_4: 6.0
	AsSe: 2.0	$AsSe_2$: 14.0	
		Ge^tSe_2: 10.0	
		Ge^tAsSe: 4.0	
Ge^t: (33 %)	—	—	100
			As_2Se_2: 32.0
			$AsSe_3$: 24.0
			$GeSe_3$: 20.0
			$GeAsSe_2$: 8.0
			Ge^tSe_3: 8.0
			Se_4: 4.0
			As_3Se: 4.0
As:	—	100.0	—
		$AsSe_2$: 32.2	
		As_2Se: 22.2	
		Ge^tAsSe: 12.2	
		As_3: 6.7	
		Se_3: 5.6	
		Ge^tAs_2: 4.4	
		Ge^tGeSe: 3.3	
		Ge^tSe_2: 3.3	
		GeAsSe: 3.3	
		$GeAs_2$: 2.2	
		Ge^tGeAs: 2.2	
		Ge^t_2Se: 1.1	
		Ge^t_2As: 1.1	
Se:	63.7	35.6	0.7
	Ge^tAs: 16.3	Ge_2As: 14.1	
	GeAs: 14.1	Ge^tGe_2: 6.7	Ge_4: 0.7
	As_2: 14.1	Ge_3: 5.9	
	Ge^tGe: 8.9	Ge^tGeAs: 3.0	
	Ge^t_2: 3.7	$GeAs_2$: 3.0	
	Ge_2: 2.2	Ge^t_2Ge: 1.5	
	AsSe: 2.2	Ge_2Se: 0.7	
	GeSe: 0.7	As_3: 0.7	
	Ge^tSe: 0.7	Ge^t_2As: 0.7	

Table SVII. Statistics of coordination environments in a-$Ge_{25}As_{30}Se_{45}$ quenched in 12 ps. The percentage of the total number of atoms of each element is given for configurations with a weight greater than 1 %.

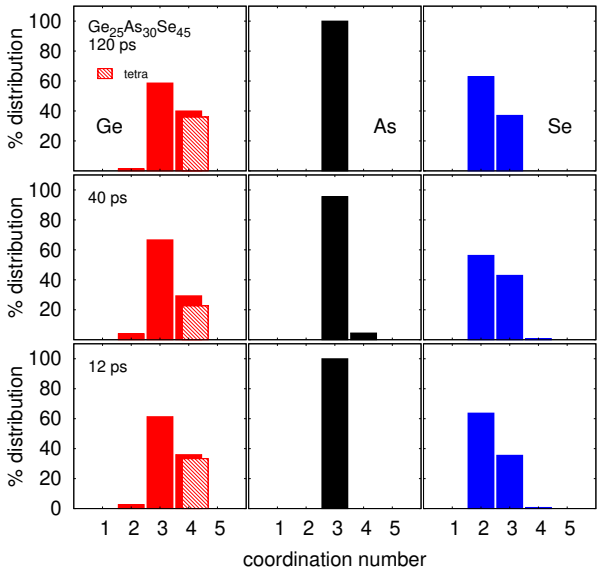

Figure S6. Distribution of coordination numbers of models of a-$Ge_{25}As_{30}Se_{45}$ generated with different quenching time.

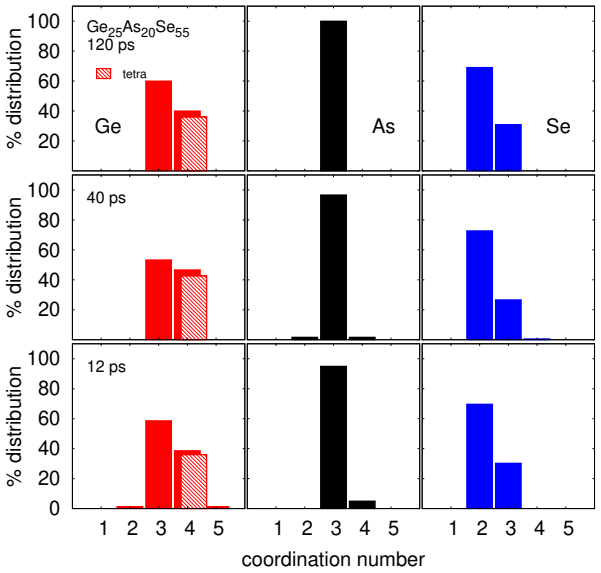

Figure S8. Distribution of coordination numbers of models of a-$Ge_{25}As_{20}Se_{55}$ generated with different quenching time.

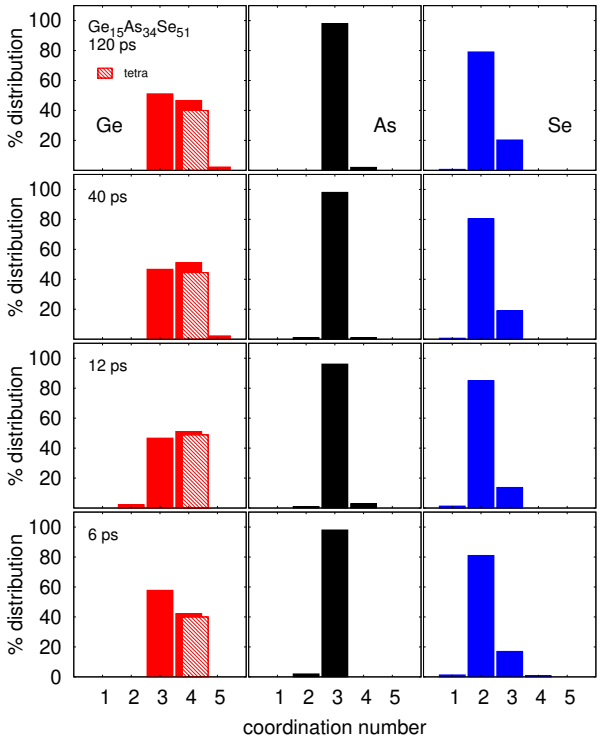

Figure S7. Distribution of coordination numbers of models of a-$Ge_{15}As_{34}Se_{51}$ generated with different quenching time.

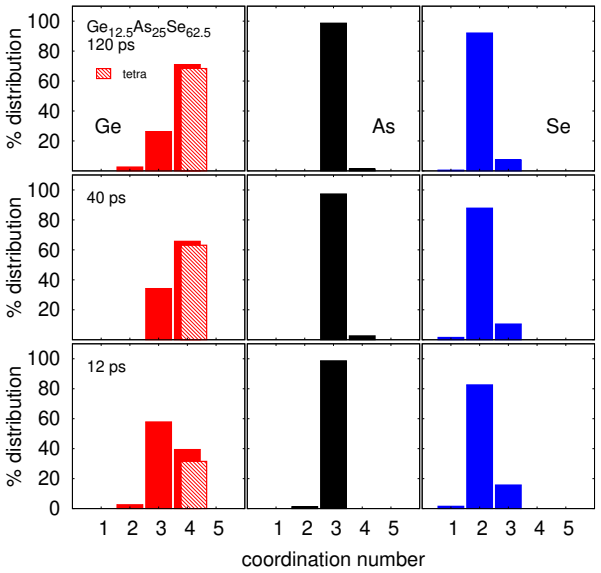

Figure S9. Distribution of coordination numbers of models of a-$Ge_{12.5}As_{25}Se_{62.5}$ generated with different quenching time.

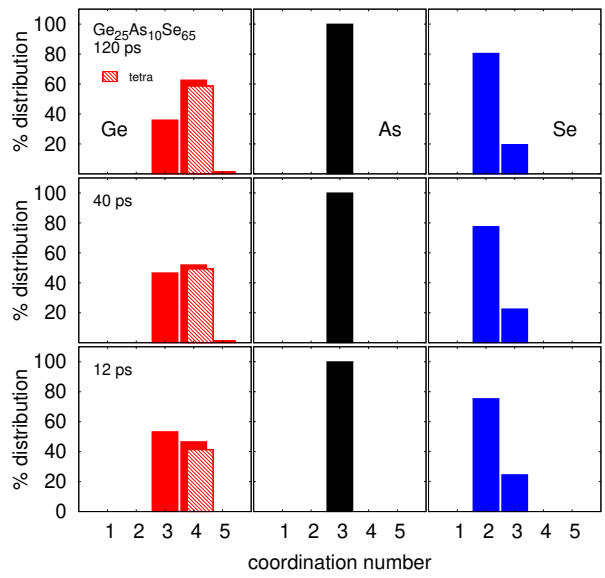

Figure S10. Distribution of coordination numbers of models of a-$Ge_{25}As_{10}Se_{65}$ generated with different quenching time.

composition	τ_q	Ge_t-As	Ge-As	ratio
$Ge_{25}As_{30}Se_{45}$	120	27 (6 %)	33 (8 %)	82 %
≫	40	17 (4 %)	26 (6 %)	65 %
≫	12	27 (6 %)	37 (9 %)	73 %
$Ge_{15}As_{34}Se_{51}$	120	17 (4 %)	21 (5 %)	81 %
≫	40	12 (3 %)	14 (3.5 %)	86 %
≫	12	21 (5 %)	23 (6 %)	91 %
≫	6	17 (4 %)	21 (5 %)	81 %
$Ge_{25}As_{20}Se_{55}$	120	14 (3 %)	14 (3 %)	100 %
≫	40	18 (4 %)	20 (5 %)	90 %
≫	12	18 (4 %)	21 (5 %)	86 %
$Ge_{12.5}As_{25}Se_{62.5}$	120	9 (2.4 %)	9 (2.4 %)	100 %
≫	40	5 (1.3 %)	5 (1.3 %)	100 %
≫	12	5 (1.3 %)	5 (1.3 %)	100 %
$Ge_{25}As_{10}Se_{65}$	120	2 (0.5 %)	2 (0.5 %)	100 %
≫	40	4 (1 %)	4 (1 %)	100 %
≫	12	4 (1 %)	5 (1 %)	80 %
$Si_{10}Ge_{15}As_{30}Se_{45}$	120	36 (5 %)	49 (7 %)	74 %
≫	40	22 (3 %)	38 (5 %)	58 %
≫	12	32 (4.5 %)	45 (6 %)	71 %

Table SVIII. Number of Ge-As bonds involving tetrahedral Ge atoms (Ge_t) and the total number of Ge-As bonds and their rato in %.

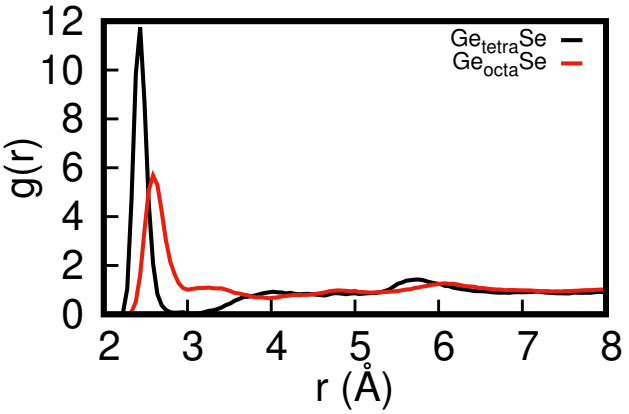

Figure S11. Ge-Se partial pair correlation function resolved for tetrahedral and octahedral/pyramidal geometries for the mq120 model of a-$Ge_{25}As_{20}Se_{55}$.

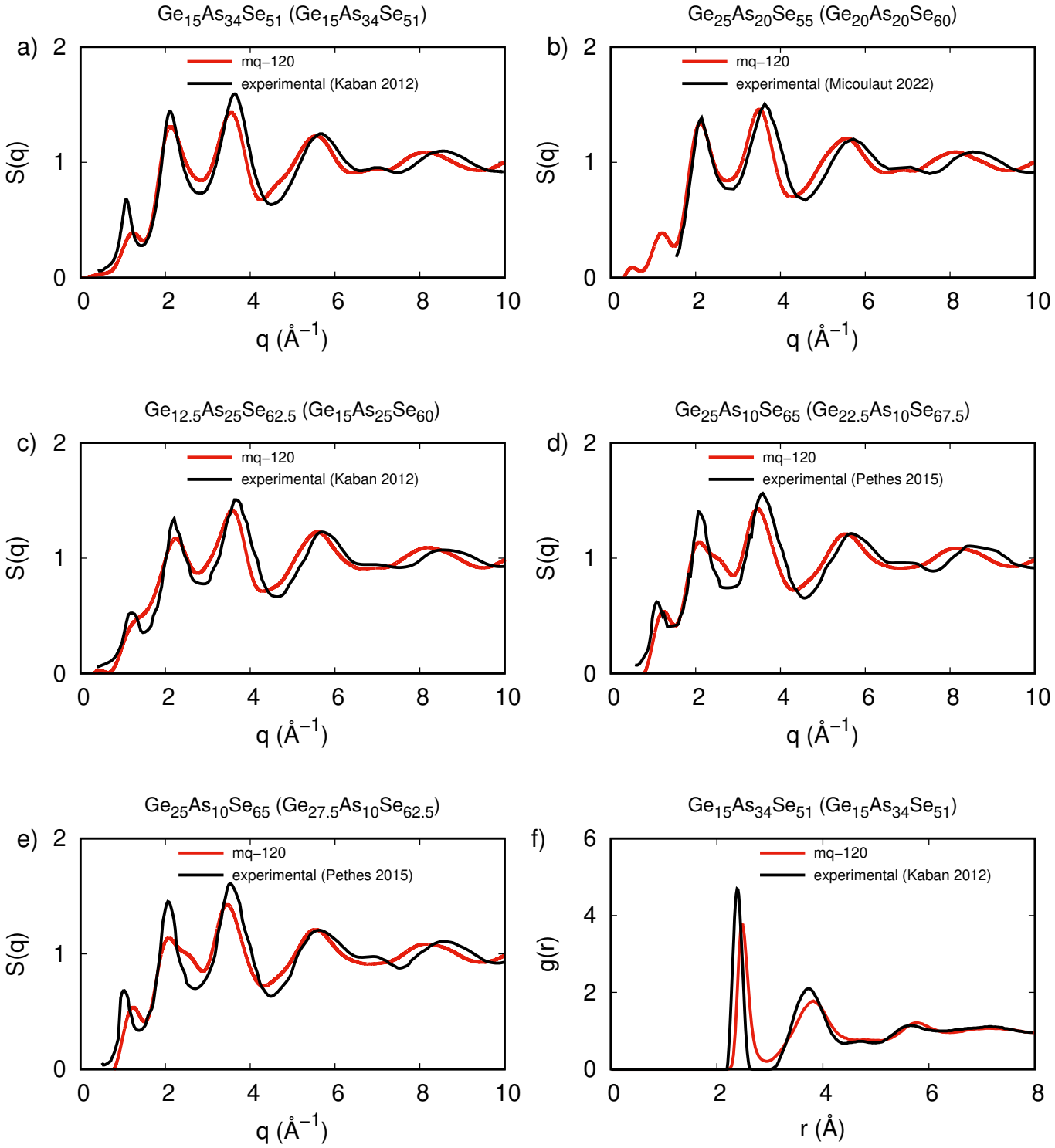

Figure S12. a)-e) Comparison of theoretical XRD structure factors of the amorphous models with experimental XRD data on similar compositions (given in parenthesis). f) Comparison between theoretical and experimental pair correlation function for the $Ge_{15}As_{34}Se_{51}$ composition. Experimental data are from Ref. [1] (Kaban 2012), Ref. [2] (Pethes 2015) and Ref. [3] (Micoulaut 2022).

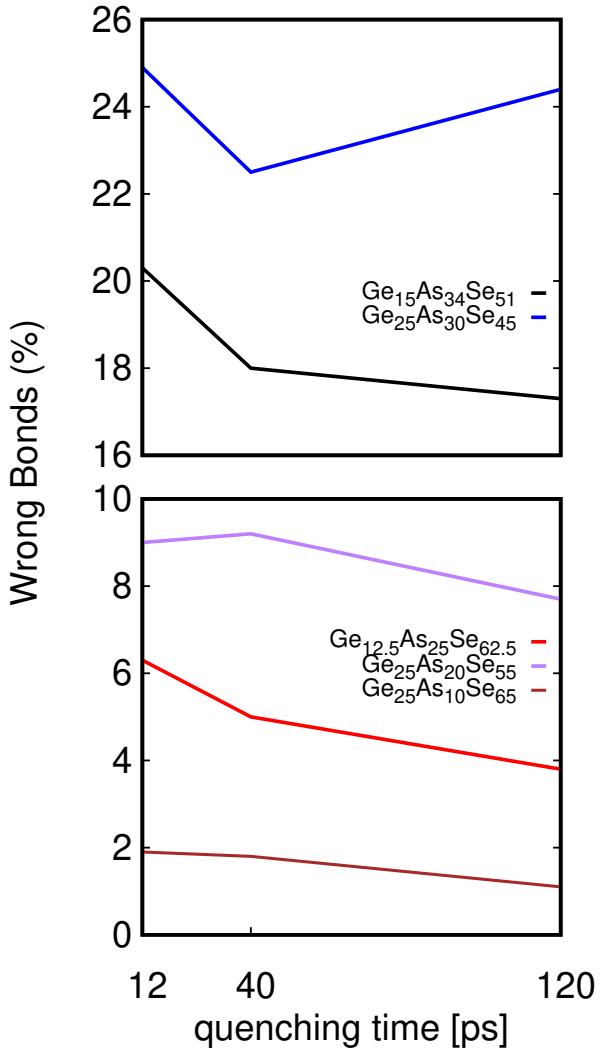

Figure S 13. Overall fraction of wrong bonds (As-As, Ge-Ge, Ge-As, Se-Se) for the models generated with different quenching time at different compositions.

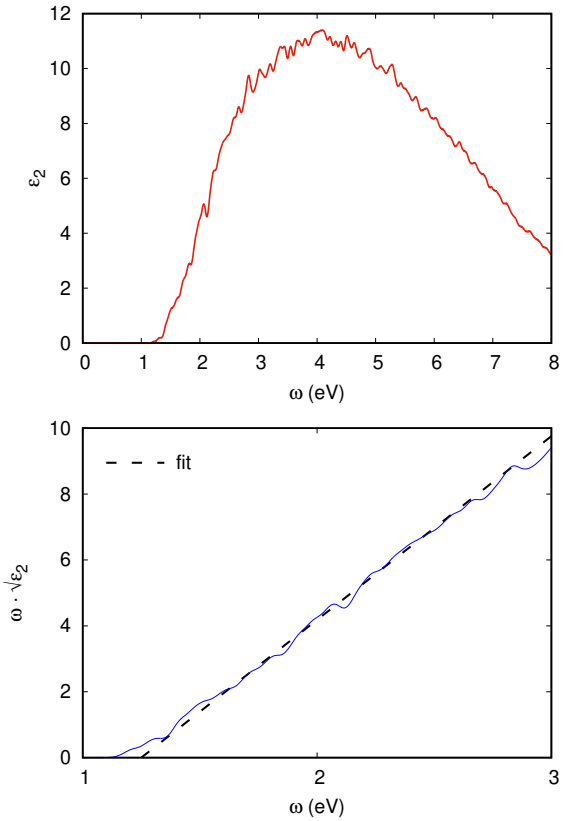

Figure S14. (Upper panel) The imaginary part of the dielectric function and (Lower panel) Tauc plot and linear fit computed for the composition $Ge_{15}As_{34}Se_{51}$ (HSE functional).

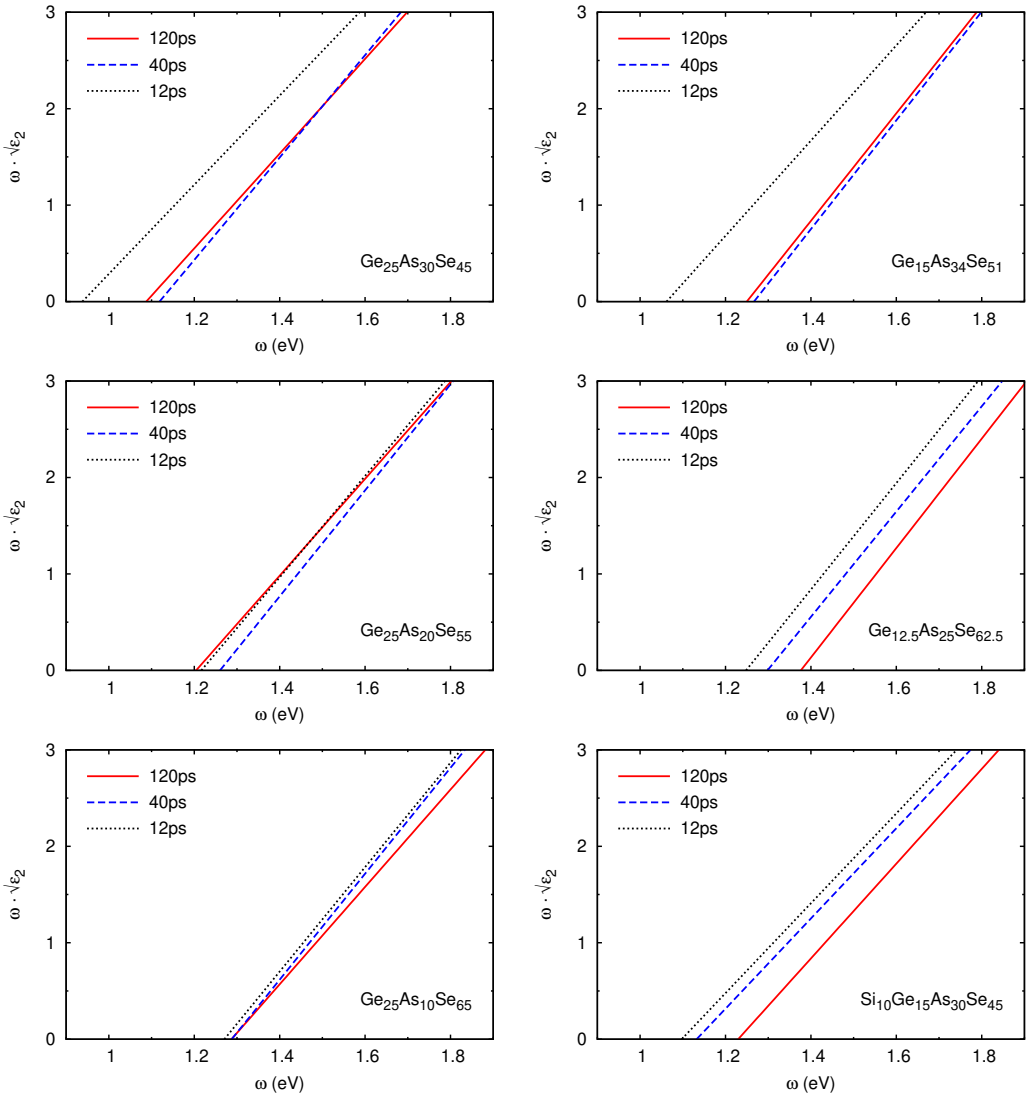

Figure S15. Linear fit to the Tauc plot for amorphous GeAsSe alloys at different compositions and for the $Si_{10}Ge_{15}As_{30}Se_{45}$ model quenched in 120, 40 and 12 ps (HSE functional).

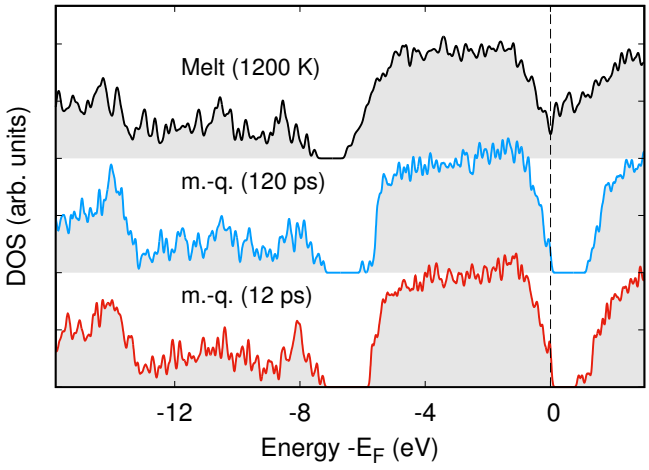

Figure S16. Electronic density of states (HSE functional) of different models (see text) of $Ge_{15}As_{34}Se_{51}$ in the liquid and amorphous phases. The zero of energy corresponds to the Fermi level in the liquid, and to the highest occupied KS state (HOMO) in the semiconducting amorphous phase. The DOS at the Fermi level in the liquid is $2 \cdot 10^{-3}$ states $Å^{-3}$ eV^{-1}.

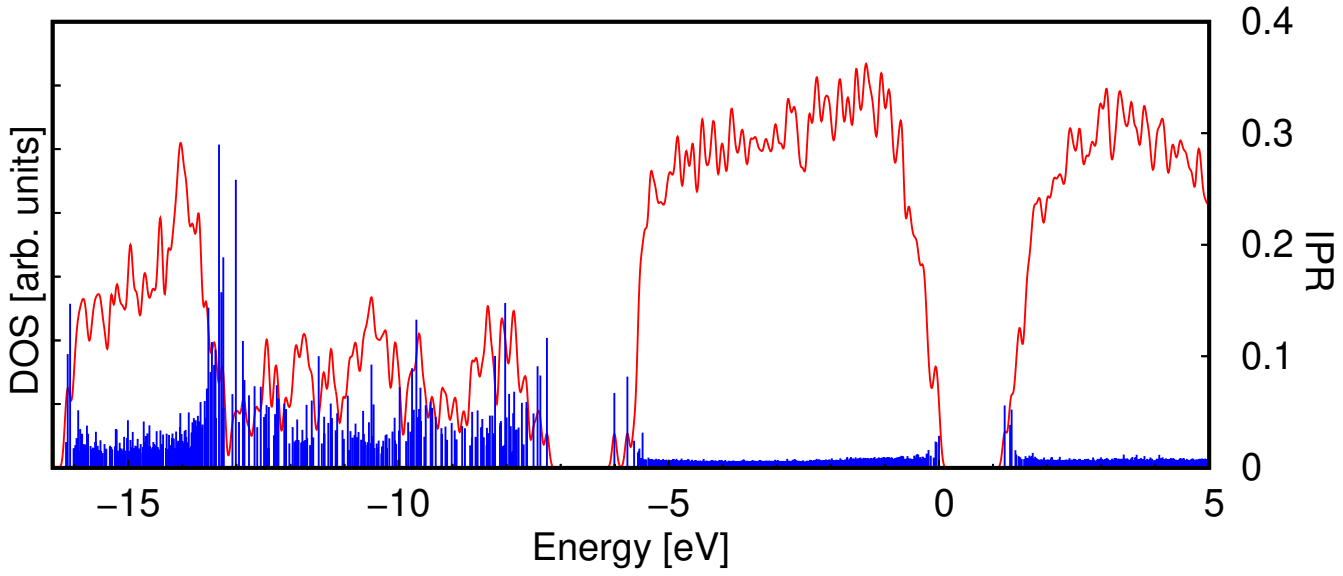

Figure S17. The DOS superimposed to the Inverse Participation Ratio (IPR, right scale) for the mq120 model of a-$Ge_{15}As_{34}Se_{51}$. The higher the IPR value the more localized is the individual Kohn-Sham state. The HSE functional is used.

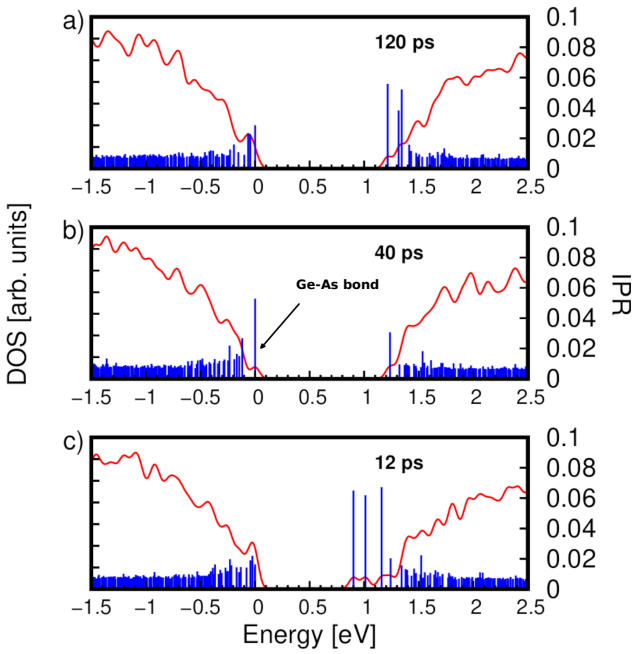

Figure S18. A zooming of the DOS close to the band gap and the values of the Inverse Participation Ratio (IPR, right scale) are shown for the models of a-$Ge_{15}As_{34}Se_{51}$ quenched in 120, 40 and 12 ps (HSE functional). The assignment of the most localized states for the mq120 and mq12 models is given in Fig. 10 in the article.

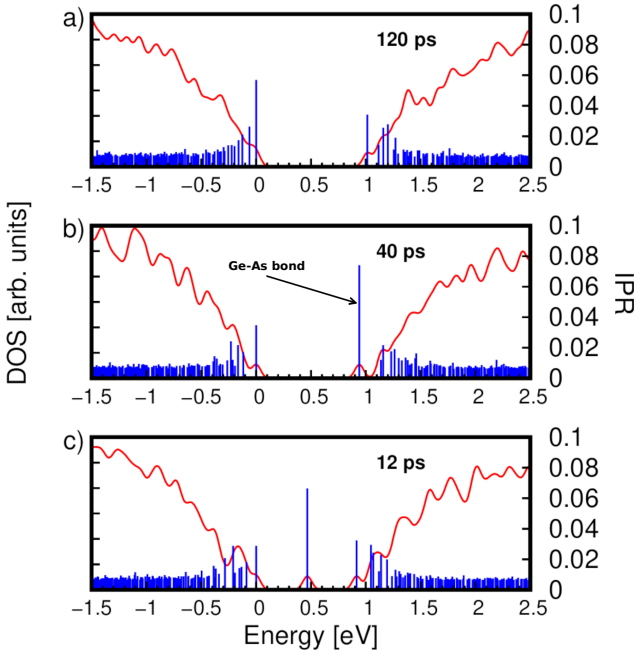

Figure S19. A zooming of the DOS close to the band gap and the values of the Inverse Participation Ratio (IPR, right scale) are shown for the models of a-$Ge_{25}As_{30}Se_{45}$ quenched in 120, 40 and 12 ps (HSE functional). The assignment of the most localized states for the mq120 and mq12 models is given given in Fig. 13 in the article.

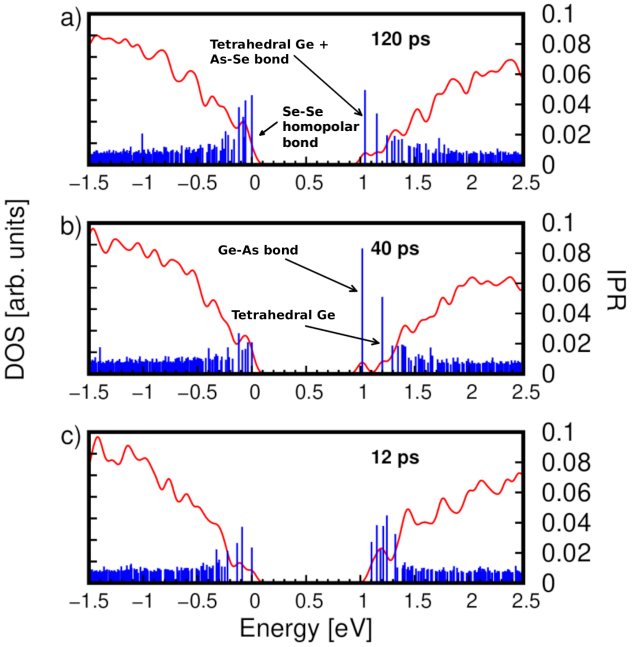

Figure S20. A zooming of the DOS close to the band gap and the values of the Inverse Participation Ratio (IPR, right scale) are shown for the models of a-$Ge_{25}As_{20}Se_{55}$ quenched in 120, 40 and 12 ps (HSE functional). The LUMO state of the mq120 model and the LUMO+1 of the mq40 model are localized on corner-sharing and isolated Ge tetrahedra respectively.

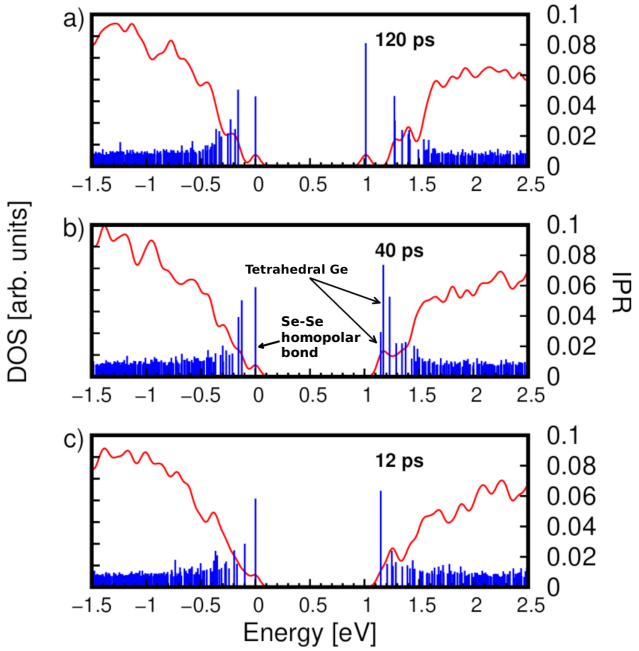

Figure S21. A zooming of the DOS close to the band gap and the values of the Inverse Participation Ratio (IPR, right scale) are shown for the models of a-$Ge_{25}As_{10}Se_{65}$ quenched in 120, 40 and 12 ps (HSE functional). The LUMO and LUMO+1 states of the mq40 model are localized on corner-sharing and edge-sharing Ge tetrahedra respectively. The assignment of the other most localized states is given in Fig. 14 in the article.

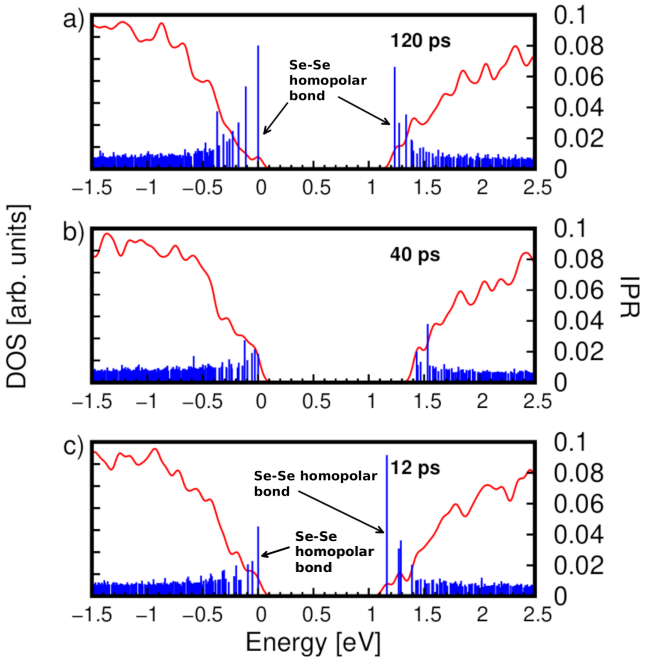

Figure S22. A zooming of the DOS close to the band gap and the values of the Inverse Participation Ratio (IPR, right scale) are shown for the models of a-$Ge_{12.5}As_{25}Se_{62.5}$ quenched in 120, 40 and 12 ps (HSE functional).

[1] I. Kaban, P. Jóvári, R. Wang, B. Luther-Davies, N. Mattern, and J. Eckert, Journal of Physics: Condensed Matter **24**, 385802 (2012).
[2] I. Pethes, I. Kaban, R.-P. Wang, B. Luther-Davies, and P. Jóvári, J. Alloys Compd. **623**, 454 (2015).
[3] M. Micoulaut, I. Pethes, P. Jóvári, L. Pusztai, M. Krbal, T. Wágner, V. Prokop, S. Michalik, K. Ikeda, and I. Kaban, Phys. Rev. B **106**, 014206 (2022).
[4] G. Opletal, R. Wang, and S. Russo, Phys. Chem. Chem. Phys. **15**, 4582 (2013).
[5] G. Opletal, R. Wang, and S. Russo, Chem. Phys. Lett. **575**, 97 (2013).